

# CrystEngComm

Accepted Manuscript



This is an *Accepted Manuscript*, which has been through the Royal Society of Chemistry peer review process and has been accepted for publication.

*Accepted Manuscripts* are published online shortly after acceptance, before technical editing, formatting and proof reading. Using this free service, authors can make their results available to the community, in citable form, before we publish the edited article. We will replace this *Accepted Manuscript* with the edited and formatted *Advance Article* as soon as it is available.

You can find more information about *Accepted Manuscripts* in the [Information for Authors](#).

Please note that technical editing may introduce minor changes to the text and/or graphics, which may alter content. The journal's standard [Terms & Conditions](#) and the [Ethical guidelines](#) still apply. In no event shall the Royal Society of Chemistry be held responsible for any errors or omissions in this *Accepted Manuscript* or any consequences arising from the use of any information it contains.

# Water Interactions in Metal Organic Frameworks

Kui Tan,<sup>†</sup> Nour Nijem,<sup>†±</sup> Yuzhi Gao,<sup>†</sup> Sebastian Zuluaga,<sup>‡</sup> Jing Li,<sup>§</sup> Timo Thonhauser,<sup>‡</sup> Yves J Chabal<sup>†\*</sup>

<sup>†</sup>Department of Materials Science & Engineering, University of Texas at Dallas, Richardson, Texas 75080

<sup>‡</sup>Department of Physics, Wake Forest University, Winston-Salem, North Carolina 27109

<sup>§</sup>Department of Chemistry and Chemical Biology, Rutgers University, Piscataway, New Jersey 08854

<sup>±</sup> Department of Chemistry, University of California Berkeley, Berkeley, California, 94720

## Abstract:

Metal organic frameworks (MOFs) have a strong potential for gas adsorption and separation process such as H<sub>2</sub> and CH<sub>4</sub> storage, and CO<sub>2</sub> capture. However, their instability in the presence of water vapor (many MOFs are hygroscopic) is one of the key issues that limit their large scale application. Previous studies of water adsorption in MOFs have mainly relied on isotherm measurements that provide useful parameters such as adsorption uptake and isosteric heat of adsorption. The structural stability of MOFs in water vapor was also evaluated by powder X-ray diffraction measurements (PXRD). However, more studies are required to unravel the water interaction or reaction mechanisms within MOFs, which would be beneficial for the development of more robust frameworks. This review highlight focuses on water adsorption in two representative MOFs: M(bdc)(ted)<sub>0.5</sub> [M = Cu<sup>2+</sup>, Zn<sup>2+</sup>, Ni<sup>2+</sup>, Co<sup>2+</sup>; bdc = 1,4-benzenedicarboxylate; ted = triethylenediamine] with saturated metal centers and MOF-74 [M<sub>2</sub>(dobdc), M = Mg<sup>2+</sup>, Zn<sup>2+</sup>, Ni<sup>2+</sup>, Co<sup>2+</sup> and dobdc = 2,5-dihydroxybenzenedicarboxylic acid] with unsaturated metal centers. It shows how vibrational spectroscopy combined with van der Waals density functional (vdW-DF) calculations make it possible to elucidate the details of water reaction in MOFs. The results presented in this highlight suggest that the reactivity and initial decomposition pathway of MOFs to water vapor critically depend on their structure and the specific metal cation in the building units. Water interaction with hydrophobic MOF, in this case FMOF-1, is also reviewed. This information provides a framework for understanding water interactions or reactions within different types of MOFs.

## 1. Introduction

Metal organic frameworks (MOFs) constitute a new family of porous materials that are attractive as adsorbent systems for gas adsorption and separation.<sup>1-6</sup> These relatively new porous materials are usually prepared through a solvothermal reaction between organic and inorganic species, and the crystalline structure contains inorganic nodes (metal ions or clusters), also referred to secondary building units (SBUs), and organic linkers, such as dicarboxylate organic rings.<sup>7, 8</sup> A wide variety of cations in the SBUs and functionalized organic linkers provides many possibilities to design the structures and tune the surface properties of the synthesized materials.<sup>9</sup> The resulting MOFs have microporous structures (pores < 2 nm) that provide high surface areas (up to 5900 m<sup>2</sup>/g) and pore volume (up to 2 cm<sup>3</sup>/g).<sup>7, 11</sup> Compared to other traditional porous materials such as aluminosilicate zeolites, carbon and metal-oxide molecular-sieves, activated carbon, activated alumina, carbon nanotubes, MOFs have unique advantages including controlled pore shape, dimensionality and tailored chemical environment.<sup>12, 13</sup> The combination

of these important features makes MOFs promising adsorbent materials for energy and environmental technologies such as H<sub>2</sub>, CH<sub>4</sub> storage and CO<sub>2</sub> capture.<sup>3, 5, 14</sup>

Despite their potential as adsorbent materials, MOFs suffer from severe issues that need to be overcome for use in practical applications.<sup>3-5</sup> The primary concern is water stability. Water could either displace the bound ligand, leading to a collapse of the MOFs structure, or block the binding sites and prevent the adsorption of other target molecules. Many widely investigated MOFs, particularly built by carboxylate acid ligand such as MOF-5,<sup>15</sup> MOF-177,<sup>16</sup> HKUST-1,<sup>17</sup> MOF-74<sup>18</sup> are water sensitive, while some zeolitic imidazolate frameworks (ZIF) materials exhibit good resistance to hydrolysis.<sup>19, 20</sup> Water stability is an issue for any application of MOFs in industrial settings because moisture is ubiquitous in the environment, i.e. complete removal of H<sub>2</sub>O from gas sources is difficult. For example, flue gas, resulting from fossil fuel combustion, is always saturated with H<sub>2</sub>O (5-7 % by volume).<sup>5, 21</sup>

Previous studies of water adsorption into MOFs rely mainly on isotherm and XRD measurements.<sup>22-25</sup> In a very recent review, Canivet and co-workers<sup>22</sup> considered water adsorption-desorption isotherms for a non-exhaustive yet representative set of MOF materials including MOF-74, UiO-66, Materials Institute Lavoisier (MILs) MOFs and proposed the three different adsorption mechanism: reversible and continuous pore-filling, through capillary condensation (irreversible and discontinuous), and irreversibility arising from the flexibility and possible structural modifications of the host material. In addition, powder X-ray diffraction (PXRD) has been an important method to check and evaluate the structural integrity after exposure to water.<sup>26-29</sup> However, both of isotherm and PXRD do not provide a molecular-level understanding of the interaction of water molecules *within* the unit cell. Therefore, detailed knowledge about bond breaking and reforming upon hydration is still sparse in the current literature.<sup>30, 31</sup>

In this highlight, we first present some examples of MOFs with low stability under water vapor in Section 2. In the follow section 3.1, 3.2 and 4.1, we focus on recent studies on the interaction of water molecules and/or the reaction mechanisms within two moisture sensitive MOFs: M(bdc)(ted)<sub>0.5</sub> and MOF-74 and one water stable fluorinated MOF: FMOF-1, based on a combination of vibrational spectroscopy (Infrared and Raman) and van der Waals density functional (vdW-DF<sup>32-35</sup>) calculations. These joint spectroscopic characterization and theoretical modeling allow us to obtain the insight into the structural variation of these two prototypical MOFs upon hydration. Finally we give some recent examples of water stable MOFs developed by other research groups in section 4.2 and 4.3 including MOF with protective groups and Zr-MOFs.<sup>36-44</sup>

## 2. Effects of water exposure on MOFs' structure stability

Due to a relatively weak coordination bond between the metal SBU and ligands, MOFs are susceptible to reaction with moisture.<sup>5</sup> Unfortunately, most of the promising MOFs adsorb significant amounts of H<sub>2</sub>O which often results in their structural collapse and a substantial decrease in their gas adsorption capacity.<sup>28</sup> For example, MOF-5 [Zn<sub>4</sub>O(bdc)<sub>3</sub>; bdc = 1,4-benzenedicarboxylates], one of the early reported MOFs, is very sensitive to water. Exposure of MOF-5 to water results in a protonation reaction of its bdc linker.<sup>15, 45</sup> Another material, MOF-177 [Zn<sub>4</sub>O(BTB)<sub>2</sub>; BTB = 4,4',4''-benzene-1,3,5-triyl-tribenzoate], which has a very high surface

area ( $> 5,000 \text{ m}^2/\text{g}$ ), quickly loses its original crystalline structure upon exposure to air (within 3 days) resulting in a drastic decrease in its surface area ( $30 \text{ m}^2/\text{g}$ ).<sup>16</sup> Figure 1 shows that some new peaks at 5-15 °C appeared after exposing to ambient air (RH~40%) for 1 day and after three days the sample became amorphous. Finally, the class of MOF described by the general formula  $M(\text{bdc})(\text{ted})_{0.5}$  [ $M = \text{Zn}, \text{Ni}$ ;  $\text{bdc} = 1,4\text{-benzenedicarboxylate}$ ;  $\text{ted} = \text{triethylenediamine}$ ], which has excellent absorbent properties for a variety of gases ( $\text{H}_2$ ,  $\text{CO}_2$ ,  $\text{CH}_4$ ,  $\text{SO}_2$ , and other hydrocarbons),<sup>46-48</sup> only remains stable in humidity levels below 30 % and fully decomposes in 60 % humidity at room temperature.<sup>49</sup> Previous hypotheses have attributed the instability of these MOFs to hydrolysis of their metal carboxylate group.<sup>26</sup>

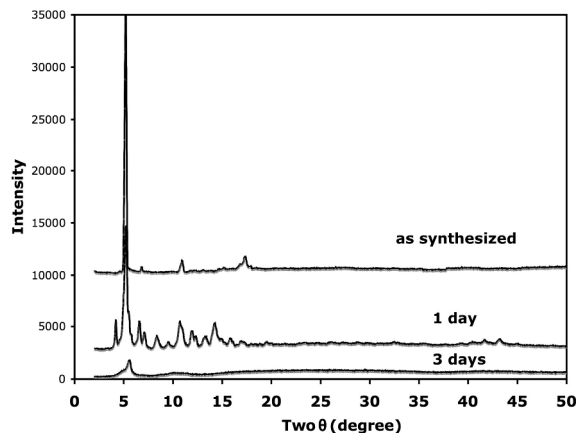


**Figure 1.** XRD patterns of the MOF-177 as synthesized and after removing guest molecules and exposing to ambient air (RH  $\sim 40\%$ ) at 298 K for 1 and 3 days. The figure is reprinted with permission from reference <sup>16</sup>. Copyright (2007) American Chemical Society.

For some MOFs, the gas uptake capacity is greatly reduced after hydration although their crystalline structure is maintained.<sup>18, 50, 51</sup> The most striking example is MOF-74 [ $M_2(\text{dobdc})$ ,  $M = \text{Mg}^{2+}, \text{Zn}^{2+}, \text{Ni}^{2+}, \text{Co}^{2+}$  and  $\text{dobdc} = 2,5\text{-dihydroxybenzenedicarboxylic acid}$ ]. MOF-74 consists of a three-dimensional honeycomb lattice with one-dimensional pores and contains a high density of coordinatively unsaturated metal sites, which are available for binding small molecules such as  $\text{CO}_2$ ,  $\text{NO}$ ,  $\text{SO}_2$ ,  $\text{CH}_4$  and  $\text{H}_2$ .<sup>14, 52-55</sup> Thermal regeneration under vacuum is sufficient to remove the adsorbed water molecules and restore the crystalline structure, even after hydration under high humidity (70 %), as evidenced by the stability of PXRD pattern. However, only 16 % of its original  $\text{CO}_2$  adsorption capacity is recovered after the hydration/regeneration process for Mg-MOF-74. The performance ( $\text{CO}_2$  adsorption capacity) of MOF-74 with other metal centers is also affected to varying degrees as shown in Figure 2. The dependence of MOF-74 and others on water remains a primary limitation for use in potential industrial applications.<sup>18</sup>

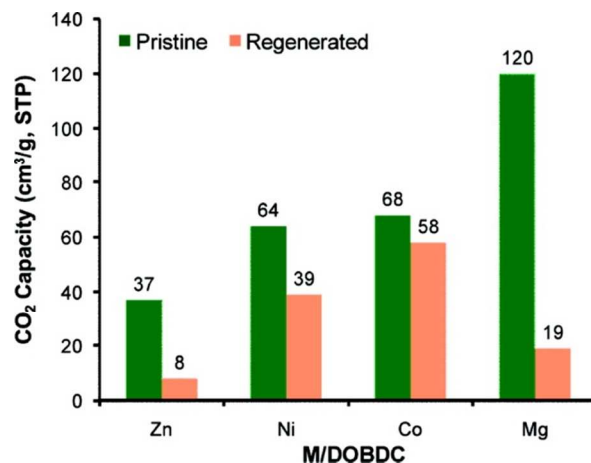
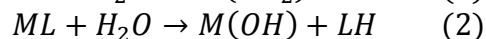
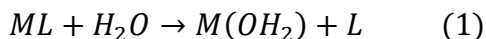


**Figure 2.** Comparison of CO<sub>2</sub> capacities of pristine MOF-74 and regenerated MOF-74 samples after hydration at 70% Relative Humidity (RH). The figure is reprinted with permission from reference <sup>18</sup>. Copyright (2011) American Chemical Society.

### 3. Degradation mechanism of MOFs in water vapor

It is important to understand the degradation mechanism by water incorporation to provide future guidance for designing and preparing water robust MOFs. For the past decade, over 20000 different MOFs have been reported and the local structure of metal nodes exhibits a rich diversity based on the self-assembly reaction and different metal coordination geometry.<sup>56</sup> Investigation of the details of water reaction mechanism with MOFs to derive some conclusive rules will be challenging and complicated. Furthermore, a structural method such as PXRD does not provide the information on the perturbations of chemical bonding during water reaction with metal-ligand node.<sup>30,31</sup> Therefore, the knowledge concerning the MOFs degradation mechanism by water vapor is rather poor. Theoretical modeling including molecular dynamics and quantum mechanical calculations have offered a promising way to unveil the detailed mechanism of water interaction with building units of MOFs and possible reaction pathways.<sup>26,45,57,58</sup>

Greathouse and Allendorf<sup>45</sup> used empirical force fields and molecular dynamics to infer that the reaction is initiated by a direct attack of MOF-5 by water molecules in the possible way: oxygen of water replaces one of ZnO<sub>4</sub> tetrahedron, leading to the release of the ligand. This ligand-displacement mechanism was also proposed by De Toni *et al.*'s modeling based first-principles calculations.<sup>57</sup> It was found that, at higher loading, a water cluster can be formed at the Zn<sub>4</sub>O site and stabilize the water-bound state. This structure rapidly transforms into a linker-displaced state, where water has fully displaced one arm of a linker. Later, Han *et al.*<sup>58</sup> used a reactive force field (ReaxFF) approach to perform a detailed study of the hydrolysis of IRMOF-1 (MOF-5), IRMOF-10, MOF-74, and found that above certain amount of loading, for instance, >4.5 wt% H<sub>2</sub>O in IR-MOF-1, the water molecules are randomly distributed in the MOF. Then, after interacting with the Zn-O moiety in an SBU, the H<sub>2</sub>O molecule dissociates into H<sup>+</sup> and OH<sup>-</sup>. The OH attaches to the Zn, while the H is attached to the oxygen atoms of the BDC. After this, the IR-MOF-1 loses its original structure and collapses. Similar results were found for MOF-74, where the MOF loses its original structure after the dissociation of the water molecules leads to the H<sup>+</sup> and OH<sup>-</sup> to bond to the O atoms of the linker and the metal centers respectively. The two mechanisms (hydrolysis or ligand displacement) are summarized by the following equations:<sup>22</sup>



These works represent the pioneering mechanistic studies of water reaction with MOFs based on theoretical modeling. In the following two sub-sections, We show how (i) *in-situ* infrared (IR) spectroscopy, (ii) *ex-situ* Raman spectroscopy, and (iii) powder X-ray diffraction, combined together with *ab initio* calculations can unveil the reaction mechanism of water molecules with the prototypical frameworks i) M(bdc)(ted)<sub>0.5</sub> based on paddlewheel type secondary building units (SBUs) and ii) MOF-74 with saturated metal centers. Infrared spectroscopy has proven to be useful in providing information about water bonding, as previously demonstrated for characterizing adsorbed water in MOF materials.<sup>59, 60</sup> Raman spectroscopy provides complementary information of the organic linkers modes to IR, and enables the characterization of metal oxide vibrational modes of the MOF that occur in the low frequency region (50-600 cm<sup>-1</sup>).<sup>59</sup> Isotopic studies using D<sub>2</sub>O are necessary to avoid interference between the infrared absorption bands of trace amount of unreacted H<sub>2</sub>bdc molecules and of H<sub>2</sub>O vapor in the spectrometer. Furthermore, in MOF-74 system, the evidence of H<sub>2</sub>O dissociation in MOF-74 is "hidden", as its experimental IR signature is overshadowed by the vibrational modes of the MOF itself. However, using D<sub>2</sub>O instead of H<sub>2</sub>O reveals an IR absorption band at 970 cm<sup>-1</sup> that gives the critical clue for the water dissociation mechanism

### 3.1 MOF with saturated metal center: M(bdc)(ted)<sub>0.5</sub> [M=Cu<sup>2+</sup>, Zn<sup>2+</sup>, Ni<sup>2+</sup> and Co<sup>2+</sup>]

M(bdc)(ted)<sub>0.5</sub> compounds are interesting because their metal node paddlewheel binuclear metal cluster are one of the most common secondary building units. These units can be found in a large number of reported MOFs with high microporosity, thermal stability and good adsorption properties.<sup>61-67</sup> Therefore, studies of the decomposition mechanisms of M(bdc)(ted)<sub>0.5</sub> are useful for evaluating a large number of MOFs' stability in water vapor. Isostructural M(bdc)(ted)<sub>0.5</sub> compounds have been prepared by incorporating different metal centers such as Cu<sup>2+</sup>, Zn<sup>2+</sup>, Ni<sup>2+</sup> and Co<sup>2+</sup>. The sorption properties for the weakly adsorbed small molecules such as H<sub>2</sub>, CO<sub>2</sub> show little dependence on the metal center since the metal ions are fully coordinated by ligands.<sup>49, 68, 69</sup> However, the stability and reaction pathway of M(bdc)(ted)<sub>0.5</sub> are in general expected to depend on the central metal ions.

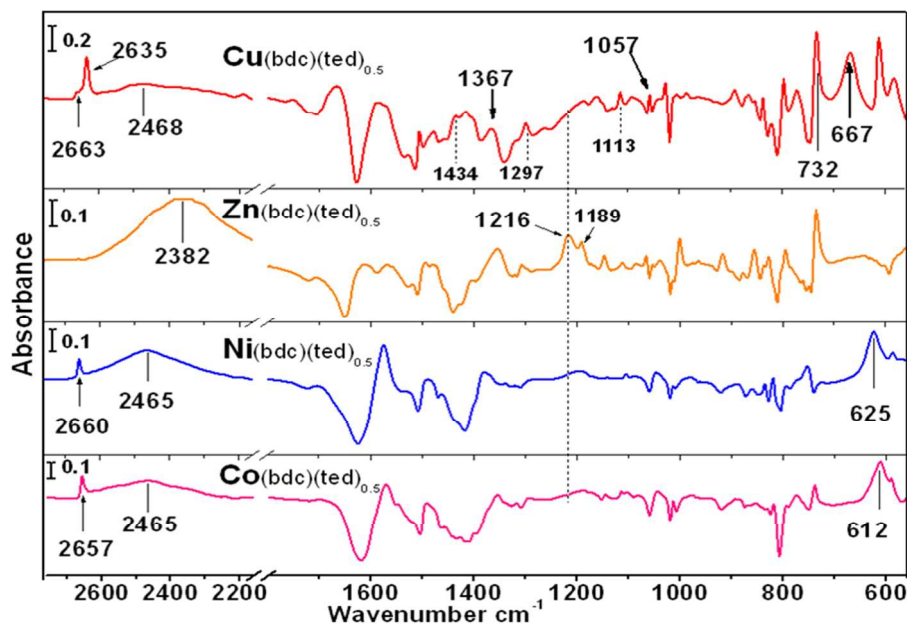


**Figure 3.** IR adsorption spectra of hydrated  $M(\text{bdc})(\text{ted})_{0.5}$ , referenced to activated MOF in vacuum after introduction of 9.5 Torr  $\text{D}_2\text{O}$  vapor and evacuation of gas phase  $\text{D}_2\text{O}$  vapor. The figure is reprinted with permission from reference <sup>30</sup>. Copyright (2012) American Chemical Society.

After exposing the activated sample to 9.5 Torr  $\text{D}_2\text{O}$  vapor for 50 min,  $\text{Cu}(\text{bdc})(\text{ted})_{0.5}$  is fully hydrolyzed by  $\text{D}_2\text{O}$  molecules. The most direct evidence is the appearance of the  $\nu(\text{O-D})$  band at  $2335\text{ cm}^{-1}$  and the weaker band at  $2663\text{ cm}^{-1}$  (see Figure 3), which can be ascribed to  $\nu(\text{CO-D})$  due to deuteration of  $\text{COO}^-$  by the  $\text{D}_2\text{O}$  molecules and to the  $\nu(\text{O-D})$  bonded to  $\text{Cu}(\text{II})$  ions, respectively.<sup>70, 71</sup> Three other readily identified absorption bands at  $1367\text{ cm}^{-1}$ ,  $1057\text{ cm}^{-1}$  and  $667\text{ cm}^{-1}$  further confirm the formation of a COOD group. The  $1367\text{ cm}^{-1}$  band are due to C-O stretching mode while the  $1057\text{ cm}^{-1}$  band and the  $667\text{ cm}^{-1}$  band of a considerable breadth are assigned to in-plane and out-of-plane OD deformation modes of dimeric carboxylic acids, which are usually in the range of  $675 \pm 25\text{ cm}^{-1}$ .<sup>72</sup> The benzene trigonal ring deformation mode represented by Wilson notation 12 appears at  $744\text{ cm}^{-1}$  in activated  $\text{Cu}(\text{bdc})(\text{ted})_{0.5}$  but shifts to  $732\text{ cm}^{-1}$  at the frequency characteristic of free bdc acid ligands.<sup>73</sup> The lineshape and position of the broad  $\nu(\text{O-D})$  are also useful to predict the different interaction of adsorbed  $\text{D}_2\text{O}$  with the MOF framework. In  $\text{Cu}(\text{bdc})(\text{ted})_{0.5}$ ,  $\text{Ni}(\text{bdc})(\text{ted})_{0.5}$ , and  $\text{Co}(\text{bdc})(\text{ted})_{0.5}$ , the stretching mode  $\nu(\text{O-D})$  is centered between  $2460$  to  $2480\text{ cm}^{-1}$  and bending mode  $\beta(\text{D-O-D})$  is centered around  $1200\text{ cm}^{-1}$ . However, in the case of  $\text{Zn}(\text{bdc})(\text{ted})_{0.5}$ ,  $\nu(\text{O-D})$  appears around  $2380\text{ cm}^{-1}$ , a distinctively lower frequency, and  $\beta(\text{D-O-D})$  develops at higher frequency ( $1216\text{ cm}^{-1}$ ). In  $\text{Ni}(\text{bdc})(\text{ted})_{0.5}$  and  $\text{Co}(\text{bdc})(\text{ted})_{0.5}$ , no clear evidence shows that carboxylate groups are hydrolyzed in these two compounds, e.g., the three characteristic bands for COOD in the region from  $1500$  to  $500\text{ cm}^{-1}$ , including C-O stretching, in plane and out-of-plane OD deformation at  $1367$ ,  $1057$ , and  $667\text{ cm}^{-1}$  are absent. Particular in  $\text{Ni}(\text{bdc})(\text{ted})_{0.5}$ , the benzene ring deformation mode  $\sigma_{12}$  remains at high frequencies with  $8\text{ cm}^{-1}$  shifts upon  $\text{D}_2\text{O}$  adsorption, which is contrary to the observation in  $\text{Cu}(\text{bdc})(\text{ted})_{0.5}$  after hydrolyzation reaction. In summary, infrared spectroscopy is very sensitive to the protonation changes of carboxylates in four  $M(\text{bdc})(\text{ted})_{0.5}$  compounds and also provides information for water adsorption state. In order to derive more details about the paddlewheel secondary building units (SBUs)  $M_2(\text{COO}^-)_4$  upon hydration and

information of the ted linker which is bonded to the apical sites of SBUs, Raman spectra were taken on both pristine and hydrated samples.

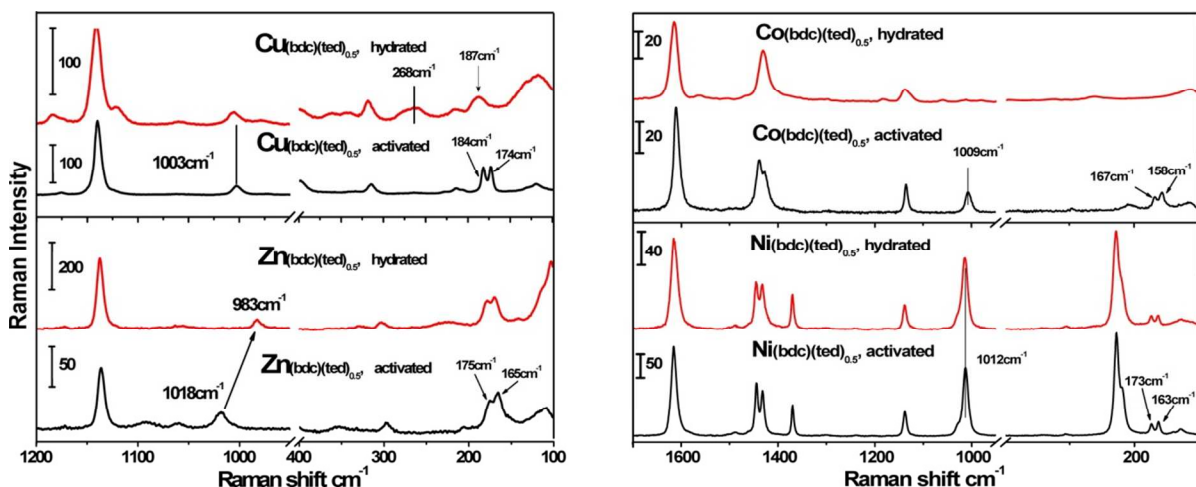


**Figure 4.** Raman spectra of activated (pristine) MOF samples and hydrated MOF materials after exposing to 9.5 Torr D<sub>2</sub>O vapor. The figure is reprinted with permission from reference <sup>30</sup>. Copyright (2012) American Chemical Society.

For Raman spectra, two main features were used to detect the structure change upon hydration: (i) A doublet appears in spectra of Cu(bdc)(ted)<sub>0.5</sub> at 184 and 174 cm<sup>-1</sup>, Zn(bdc)(ted)<sub>0.5</sub> at 175 and 165 cm<sup>-1</sup>, Ni(bdc)(ted)<sub>0.5</sub> at 173 and 163 cm<sup>-1</sup> and Co(bdc)(ted)<sub>0.5</sub> at 167 and 158 cm<sup>-1</sup> (see Figure 4). The similar doublet modes were also observed in other paddlewheel MOFs such as Cu(bdc)(dmf),<sup>30</sup> Zn(bdc)(dmf),<sup>30</sup> and Cu-btc compounds<sup>74</sup> and copper acetate monohydrate Cu(OAc)<sub>2</sub>(H<sub>2</sub>O)<sub>2</sub> around 200-160 cm<sup>-1</sup>.<sup>75</sup> The doublet in these compound is attributed to be the unique feature of di-nuclear paddle wheel building units.<sup>30</sup> According to Prestipino's resonance Raman measurement,<sup>74</sup> it most likely involves M-M stretching of the two M(II) ions of M<sub>2</sub>[COO]<sub>4</sub> framework cage. (ii) There is another marked band for triethylenediamine molecules, ν<sub>4</sub>, ν<sub>CC</sub>/ω(CH<sub>2</sub>) that involves a substantial amount of C-C stretching vibration.<sup>76-78</sup> The mixing of the nitrogen lone pair molecule orbitals with C-C molecule orbitals makes the ν<sub>4</sub> (ν<sub>CC</sub>/ωCH<sub>2</sub>) mode frequency extremely sensitive to the changes in the environment of the lone pairs.<sup>30</sup> ν<sub>4</sub> is found at 983 cm<sup>-1</sup> for the unprotonated species of ted.<sup>76</sup> Upon coordination to metal ions Cu<sup>2+</sup>, Co<sup>2+</sup>, Ni<sup>2+</sup>, Zn<sup>2+</sup> in four M(bdc)(ted)<sub>0.5</sub> compounds, this band blue shifts to 1003 cm<sup>-1</sup>, 1009 cm<sup>-1</sup>, 1012 cm<sup>-1</sup>, and 1018 cm<sup>-1</sup>.<sup>30</sup>

After exposing the activated sample to 9.5 Torr D<sub>2</sub>O vapor, the Raman spectra of hydrated M(bdc)(ted)<sub>0.5</sub> [M=Cu<sup>2+</sup>, Zn<sup>2+</sup>, Ni<sup>2+</sup> and Co<sup>2+</sup>] show marked changes compared to that of pristine sample (see Figure 4). For Cu(bdc)(ted)<sub>0.5</sub>, the doublet mode around 174 to 184 cm<sup>-1</sup> vanishes, and is replaced by a single broad peak at 187 cm<sup>-1</sup>. The hydration process leads to the formation of a mode at ~ 268 cm<sup>-1</sup>, which corresponds to the adsorption band of H<sub>2</sub>bdc.<sup>30</sup> These changes are consistent with IR observation that carboxylate group of bdc linker is protonated upon hydration. In the frequency region from 950 to 1100 cm<sup>-1</sup>, the C-C stretching mode ν<sub>4</sub> is left unchanged at 1003 cm<sup>-1</sup>, indicating that nitrogen atoms of ted linker still maintain the coordination to the Cu<sup>2+</sup> upon hydration. For Zn(bdc)(ted)<sub>0.5</sub>, the doublet mode associated with the Zn-Zn bonding persists, indicating that the paddle wheel structure remain unbroken by D<sub>2</sub>O molecules. However, the ν<sub>4</sub> mode at 1018 cm<sup>-1</sup> in the activated structure red shifts by 35 cm<sup>-1</sup> to

983  $\text{cm}^{-1}$  after hydration, suggesting that the nitrogen atom of the ted molecules is no longer connected to the metal atoms and in the unprotonated form. For  $\text{Ni}(\text{bdc})(\text{ted})_{0.5}$ , the Raman spectra do not significantly change upon hydration, suggesting that the paddlewheel structure maintains its original structure. For  $\text{Co}(\text{bdc})(\text{ted})_{0.5}$ , both the  $\nu_4$  and the doublet modes disappear after hydration, indicating the structure is strongly affected.

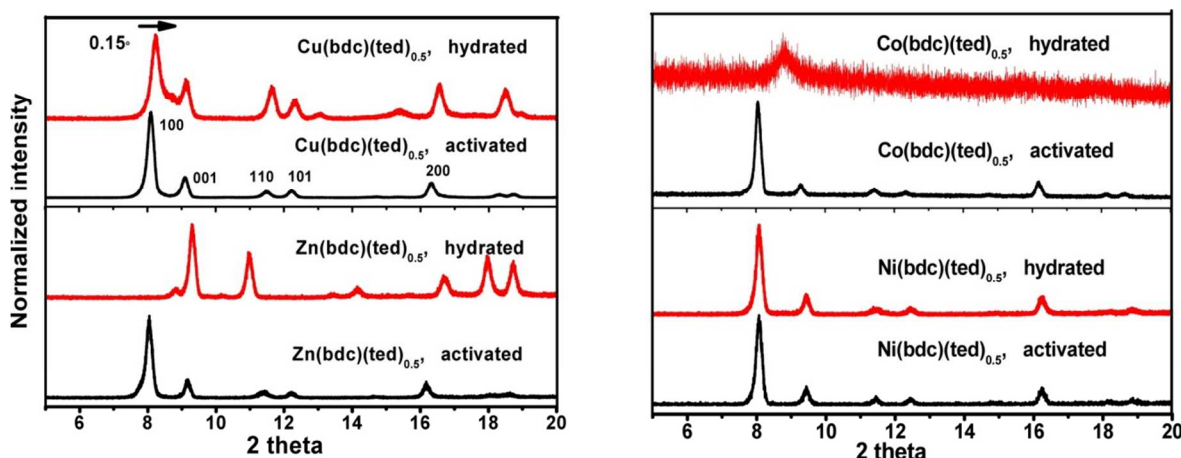


**Figure 5.** Powder X-ray diffraction pattern of hydrated MOF materials exposing to 9.5 Torr  $\text{D}_2\text{O}$  vapor and activated (pristine) MOF samples. The figure is reprinted with permission from reference<sup>30</sup>. Copyright (2012) American Chemical Society.

Powder X-ray diffraction measurements in Figure 5 show that, after hydration, all the phases except [001] shift to a higher  $2\theta$  value in  $\text{Cu}(\text{bdc})(\text{ted})_{0.5}$ , indicating that the distance between the 2D  $\text{Cu}_2(\text{COO})_4$  layers remains unchanged, which is consistent with the Raman observation that ted still coordinates to the metal sites after hydration. The position of the two-theta marks is ruled by the length of the bdc linker. Furthermore, these marks shift position when the linker is deuterated upon exposure to  $\text{D}_2\text{O}$ , which is in line with IR results that carboxylate group in the bdc linker is hydrolyzed. For  $\text{Zn}(\text{bdc})(\text{ted})_{0.5}$ , the framework undergoes a phase transition after exposure to 9.5 Torr  $\text{D}_2\text{O}$  vapor for 1h to MOF-2 [ $\text{Zn}(\text{bdc})(\text{H}_2\text{O})$ ] structure as evidenced by several characteristic peaks in Figure 5. On the other hand, MOF-2 contain the similar square-grid  $\text{Zn}_2(\text{bdc})_2$  composed of di-nuclear paddlewheel Zn-Zn units bridged by bdc di-anions. The difference is that the square-grid layers of  $\text{Zn}_2(\text{bdc})_2$  are held together by hydrogen bonding between water and two adjacent paddlewheels, with the oxygen of  $\text{H}_2\text{O}$  bound to the Zn atom and the H of the same  $\text{H}_2\text{O}$  molecule bound to the carboxylate oxygen of the adjacent paddlewheel structure.<sup>79, 80</sup> During the transformation of  $\text{Zn}(\text{bdc})(\text{ted})_{0.5}$  to MOF-2, the ted molecule is detached and water is attached to  $\text{Zn}^{2+}$  apical sites of the paddle wheel building units through their oxygen atoms. The stronger deuterium bonding of the  $\text{D}_2\text{O}$  molecules within  $\text{Zn}(\text{bdc})(\text{D}_2\text{O})$  explains the  $\nu(\text{O}-\text{D})$  band center shifts to lower wavenumber ( $\sim 2382 \text{ cm}^{-1}$ ) and the  $\delta(\text{D}-\text{O}-\text{D})$  band shifts to a higher wavenumber ( $\sim 1216 \text{ cm}^{-1}$ ) in Figure 3. Similar to Raman spectra, the powder X-ray diffraction pattern for  $\text{Ni}(\text{bdc})(\text{ted})_{0.5}$  is not affected at all by hydration, further confirming that the crystal structure, upon hydration by 9.5 Torr  $\text{D}_2\text{O}$ , remains intact. The sharp band at  $2360 \text{ cm}^{-1}$  in Figure 3 could be due to isolated adsorbed  $\text{D}_2\text{O}$  coordinating to the two Ni atoms in paddlewheel units of  $\text{Ni}(\text{bdc})(\text{ted})_{0.5}$ .<sup>30</sup> In contrast to  $\text{Ni}(\text{bdc})(\text{ted})_{0.5}$ , the crystal structure of  $\text{Co}(\text{bdc})(\text{ted})_{0.5}$  is completely destroyed after exposure to 9.5 Torr  $\text{D}_2\text{O}$  vapor, even though there is no clear evidence that carboxylate group is protonated

by hydration. However, the loss of the  $\nu_4$  mode and doublet mode at 158 and 167  $\text{cm}^{-1}$  in the Raman spectra of Figure 4, indicates that the coordinated ted linkers disappear and the Co-Co structure is affected by hydration. We conclude that  $\text{D}_2\text{O}$  molecules attack the Co-N bond and replace the ted linker, binding to the apical Co(II) site. As a result, the paddle wheel  $\text{Co}_2(\text{COO})_4$  is distorted and the Co-Co interaction is removed. The sharp peak at 2357  $\text{cm}^{-1}$  observed in IR spectra is therefore due to  $\text{D}_2\text{O}$  molecules bonded to the distorted paddle wheel  $\text{Co}_2(\text{COO})_4$  structure.

In summary, combined *in-situ* IR spectroscopy, Raman, and powder X-ray diffraction measurements show that the stability and modification of isostructural  $\text{M}(\text{bdc})(\text{ted})_{0.5}$  compounds upon exposure to water vapor critically depend on the central metal ions (see Figure 6). A hydrolysis reaction of water molecules with Cu–O–C is observed in the case of  $\text{Cu}(\text{bdc})(\text{ted})_{0.5}$ . Displacement reactions of ted linkers by water molecules are identified in  $\text{Zn}(\text{bdc})(\text{ted})_{0.5}$  and  $\text{Co}(\text{bdc})(\text{ted})_{0.5}$ . In contrast,  $\text{Ni}(\text{bdc})(\text{ted})_{0.5}$  is less susceptible to reaction with water vapor than the other three compounds. This finding can be justified by considering the metal–oxygen strength from the dissociation energy for diatomic molecules: Zn–O (~250.4 kJ/mol), Cu–O (~287.4 kJ/mol), Ni–O (~366 kJ/mol), and Co–O (~397.4 kJ/mol) and the overall formation (stability) constant of the hexaaminemetal complex in aqueous solution:  $\text{Ni}(\text{NH}_3)_6^{2+}$  ( $2.0 \times 10^8$ ) >  $\text{Co}(\text{NH}_3)_6^{2+}$  ( $2.0 \times 10^4$ );  $\text{Cu}(\text{NH}_3)_4^{2+}$  ( $1.1 \times 10^{13}$ ) >  $\text{Zn}(\text{NH}_3)_4^{2+}$  ( $2.8 \times 10^9$ ).<sup>81, 82</sup> The higher Ni–O and Ni–N bond strengths prevent bdc or ted moieties in paddlewheel  $\text{Ni}_2[\text{COO}]_4$  building units from being deuterated or displaced by  $\text{D}_2\text{O}$  molecules under the same condition of 9.5 Torr vapor exposure at RT. Although both Zn–O and Zn–N bonds are weak, the Zn–N bonds are more easily broken by reaction with  $\text{D}_2\text{O}$  molecules so that ted molecules are released from the apical sites of  $\text{Zn}_2[\text{COO}]_4$  clusters and the  $\text{D}_2\text{O}$  molecules bond to Zn SBUs. vdW-DF simulations have found that the energy ( $\Delta E$ ) required to replace the ted units with water molecules in  $\text{Zn}(\text{bdc})(\text{ted})_{0.5}$  is much lower (43.1  $\text{kJ mol}^{-1} \text{ cell}^{-1}$ ) than and in  $\text{Ni}(\text{bdc})(\text{ted})_{0.5}$ , which is 85.5  $\text{kJ mol}^{-1} \text{ cell}^{-1}$  when only two water molecules (per cell) are introduced.<sup>30</sup> Upon loading four water molecules per unit cell, the hydration of  $\text{Zn}(\text{bdc})(\text{ted})_{0.5}$  becomes spontaneous with a  $\Delta E$  of  $-5.3 \text{ kJ mol}^{-1} \text{ cell}^{-1}$ .

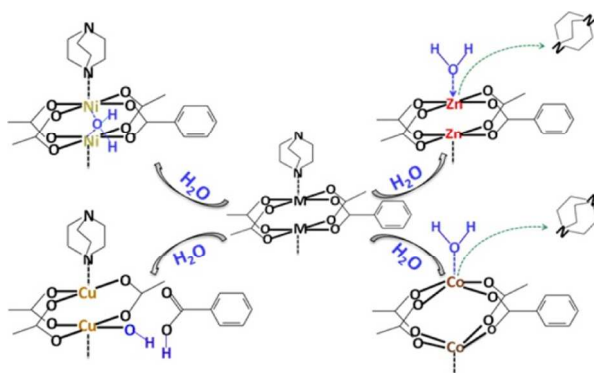


**Figure 6.** Schematic illustration of the decomposition pathways for the  $\text{M}(\text{bdc})(\text{ted})_{0.5}$  [ $\text{M}=\text{Cu}$ ,  $\text{Zn}$ ,  $\text{Ni}$ ,  $\text{Co}$ ] reaction with  $\text{H}_2\text{O}$  molecules. The figure is reprinted with permission from reference<sup>30</sup>. Copyright (2012) American Chemical Society.

### 3.2 MOFs with unsaturated metal center: M-MOF-74 ( $\text{M}=\text{Zn}^{2+}$ , $\text{Mg}^{2+}$ , $\text{Ni}^{2+}$ , $\text{Co}^{2+}$ )

MOF-74 is a member of the best studied family of MOFs with unsaturated metal centers. Its open metal sites exhibit enhanced affinities to small molecules such as  $\text{CO}_2$ ,  $\text{H}_2$ ,  $\text{CH}_4$ .<sup>14, 83, 84</sup> In fact, Mg-MOF-74 has the highest low-pressure gravimetric and volumetric adsorption capacities for  $\text{CO}_2$  of all reported MOFs.<sup>5</sup> It is therefore important to understand the stability of these

materials in moisture. The difficulty in doing so was based on the fact that, although gas uptake decreased significantly upon hydration and subsequent thermal regeneration, X-ray diffraction did not detect the significant changes.<sup>18</sup> The structure did not appear compromised, but water seemed to have altered the internal chemical composition.

At room temperature, water pressure dependence measurements suggest that water is molecularly adsorbed into MOF-74 compounds without hydrolyzing the frameworks and can be gradually removed by annealing in vacuum.<sup>85</sup> IR measurements also indicate that H<sub>2</sub>O incorporation brings in strong perturbations to MOFs phonon modes such as stretching modes of carboxylate  $\nu_{as,s}(\text{COO}^-)$ , phenolate group  $\nu(\text{C-O})$ , bending modes  $\beta(\text{CH})$ , suggesting that the water molecules do interact with MOF-74 compounds. This is supported by DFT calculations that show that water binds more strongly to open metal sites (Zn, 73.9 kJ mol<sup>-1</sup>; Mg, 73.2 kJ mol<sup>-1</sup>; Co, -71.7 kJ mol<sup>-1</sup>; Ni, 60.6 kJ mol<sup>-1</sup>) than other molecules such as CO<sub>2</sub>, CH<sub>4</sub> and H<sub>2</sub>.<sup>86</sup> However, these perturbations disappear after annealing in vacuum, which is consistent with a reversible removal of all adsorbed water molecules.

In contrast, we have recently shown<sup>85</sup> that a hidden water dissociation reaction takes place at temperatures above 150 °C and the reaction product can be only detected by using D<sub>2</sub>O vapor exposure (not H<sub>2</sub>O). A detailed analysis of (Mg, Zn, Ni, Co)-MOF-74 exposed to H<sub>2</sub>O and D<sub>2</sub>O at 100 °C, 150 °C and 200 °C reveals that a distinctive absorption band appears at ~970(6) cm<sup>-1</sup> in all four MOFs but only upon D<sub>2</sub>O exposure (i.e. there is no corresponding band at ~1332 cm<sup>-1</sup>), as summarized in Figure. 7 (top two spectra for Zn-MOF-74). This mode is clearly due to a deuterium vibration and unsaturated metal ions are effectively involved in the reaction to generate this band. Surprisingly, the counterpart hydrogen band is not detected in difference IR spectra.

To investigate this system in more detail, CO<sub>2</sub> was introduced to test the adsorption capacity of Zn-MOF-74 by *in-situ* spectroscopic measurement after H<sub>2</sub>O and D<sub>2</sub>O exposures.<sup>85</sup> The amount of CO<sub>2</sub> adsorbed decreased by 60% in both cases, suggesting that similar reactions occur within MOF-74 for both H<sub>2</sub>O and D<sub>2</sub>O. Yet, the MOF structure is not perturbed after water exposure measurement since there are no observable changes in Raman spectra and XRD pattern after D<sub>2</sub>O exposure.<sup>85</sup>

A comparison between the difference spectra of H<sub>2</sub>O, D<sub>2</sub>O exposed Zn-MOF-74 to the IR absorption spectra of activated MOF-74 shown Figure 7 (bottom spectrum) gives a clue as to the origin of this D<sub>2</sub>O-induced mode at ~970 cm<sup>-1</sup> and the corresponding hydrogen mode.<sup>85</sup> While the vibrational mode at ~970 cm<sup>-1</sup> falls in the phonon gap of the MOF vibrational spectrum, the hydrogen mode is expected to be ~1333 cm<sup>-1</sup> by a simple harmonic oscillator approximation: the vibrational frequency is proportional to  $\frac{1}{\sqrt{\mu}}$  (where  $\mu$  is the reduced mass). However, the frequency 1333 cm<sup>-1</sup> is in a spectral region where the MOF has a high phonon density. This leads to strong vibrational coupling and make it difficult to detect.

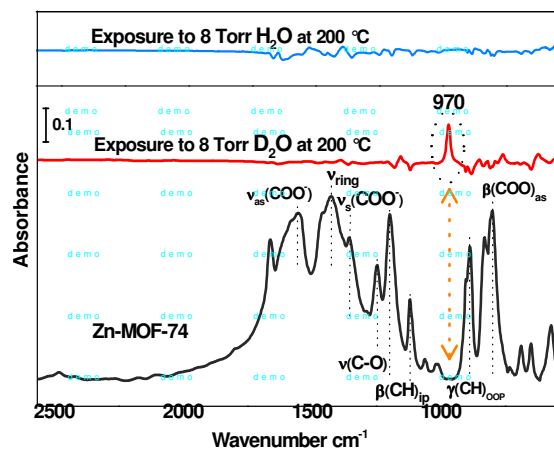


**Figure 7.** Difference spectra of H<sub>2</sub>O (blue), D<sub>2</sub>O (red) exposed Zn-MOF-74 reference to the activated MOFs, compared with the IR absorption spectra of activated MOF-74 referenced to KBr pellet. The spectra contain the selected assignment of MOF phonon modes. The content of this figure is taken from reference <sup>85</sup>. Reproduced from paper submitted to JACS and on acceptance copyright shall be assigned to the American Chemical Society.

These considerations have been validated by *ab initio* calculations.<sup>85</sup> In these calculations, we first considered all potential configurations of molecular adsorbed water (H<sub>2</sub>O, D<sub>2</sub>O) and possible dissociated products (OH, OD, H and D) directly bonded to the metal center in Zn-MOF-74 without success: none of them matched the observed frequency around the 970 cm<sup>-1</sup> mark.<sup>85</sup> The interaction of H and D atoms with the neighboring oxygen sites of the dobdc linker was then examined, finding a vibrational mode associated with the OD bending (see Figure 8a) with a frequency of 950 cm<sup>-1</sup> (when the D atom is bonded to oxygen of phenolate group). More interestingly, when this D is replaced by H, a similar mode with strong H bending movement can be found at 1317 cm<sup>-1</sup> (see Figure 8b). However, this mode also involves the strong displacement of the other atoms (C and H) of the dobdc linker. Furthermore, there is a vibrational mode in the pristine Zn-MOF-74 with same frequency (1317 cm<sup>-1</sup>). Consequently, this OH mode is strongly coupled to the pristine MOFs vibrations and therefore its vibrations cannot be detected as a strong and sharp mode.

Our DFT calculations also provided a pathway for water (H<sub>2</sub>O, D<sub>2</sub>O) dissociation:<sup>85</sup> a water molecule first attaches the unsaturated metal sites by oxygen atom. After this, the hydrogen or deuterium atom rotates and establishes a hydrogen bond with the oxygen of phenolate group. After overcoming a kinetic barrier of 1.01 eV (i.e. thermal activation necessary), the hydrogen or deuterium is abstracted by the oxygen of phenolate group, giving rise to the absorption band at ~970 cm<sup>-1</sup> in the case of D<sub>2</sub>O, and a broader mixed mode in the case of H<sub>2</sub>O.

In summary, the weak link for MOF-74 is the dobdc-metal bond.<sup>85</sup> The water molecule is dissociatively adsorbed at the metal-oxygen group with the OH adsorbed directly on the metal center and the H adsorbed on the bridging O of the phenolate group in the dobdc linker. The reactivity is highly dependent on the central metal ions of MOF-74 compounds and follows the trend: Co < Ni < Mg < Zn. Due to the passivation of the unsaturated metal sites by hydroxyl group, the gas uptake such as CO<sub>2</sub> is decreased. This finding provides insight into the long lasting question of MOF-74 degradation issues.

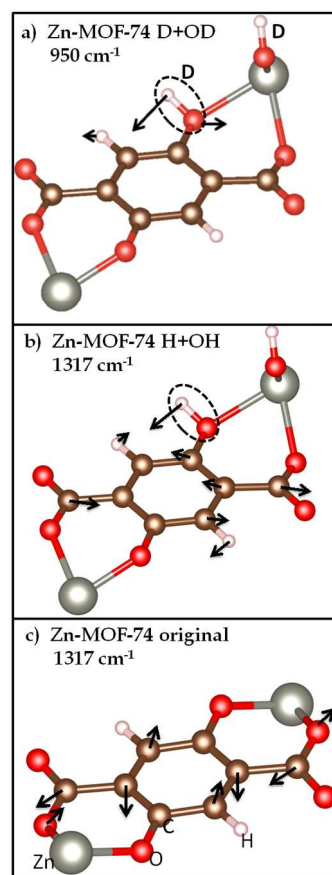


**Figure 8.** Calculated vibrational modes of (a) Zn-MOF-74 with dissociated D<sub>2</sub>O (D + OD) at 950 cm<sup>-1</sup>; (b) with dissociated H<sub>2</sub>O (H + OH) at 1317 cm<sup>-1</sup>; (c) original MOF structure at 1317 cm<sup>-1</sup>. The black arrows represent the vibration mode. The figure is taken from reference<sup>85</sup>. Reproduced from paper submitted to JACS and on acceptance copyright shall be assigned to the American Chemical Society.

#### 4. Development of water stable MOFs

By investigating water reaction with two well-known MOFs: M(bdc)(ted)<sub>0.5</sub> and MOF-74, the weakest point within MOFs is confirmed to be metal-ligand bond, which could be hydrolyzed or displaced by water molecules. This section discusses the routes implemented to enhance MOFs moisture stability. The two main approaches to tackle the stability of MOFs have focused on either modification of the linkers to have a hydrophobic character, such as the case of FMOF-1,<sup>38</sup> or enhancing the metal-linker bond by changing the metal center for example using zirconium instead of the copper or zinc.<sup>37</sup> An alternative approach explored is installing protective groups to prevent access of the water to the metal center, albeit on the cost of surface area.<sup>39, 40, 87</sup> It is worthy to mention that MOFs with enhanced water stability can be fully explored for many other applications such as water confinement, dehumidification, thermal batteries, and delivery of drinking water.<sup>22, 25, 88</sup>

##### 4.1. Hydrophobic cavities using fluorinated linker: FMOF-1

To enhance the stability of MOFs under humid conditions, one approach has been to make the pores hydrophobic to prevent framework degradation by water and prevent hydrolysis and a decrease in active surface area.<sup>41, 88</sup> For example, fluorinated metal organic frameworks are a new

class of porous materials with fluorine coated channels free of hydrogen. The presence of hydrophobic groups in the channels enhances their stability and gives them favorable adsorption properties.<sup>36, 38</sup> FMOF-1 is constructed from silver (I) 3,5-bis (trifluoromethyl)-1,2,4-triazolate (AgTz) (see Figure 9a). The framework has large ( $12.2 \text{ \AA} \times 7.3 \text{ \AA}$ ) interconnected tubes with hydrophobic cavities coated with  $\text{CF}_3$  groups of the perfluorinated ligands. The walls of each channel of the framework consist of small cavities or “cages” ( $6.6 \text{ \AA} \times 4.9 \text{ \AA}$ ) that are accessible to dynamic adsorption of small guest molecules. Water adsorption isotherms shown Figure 9b illustrates the hydrophobic nature of FMOF-1 as compared to BPL Carbon and Zeolite-5A.

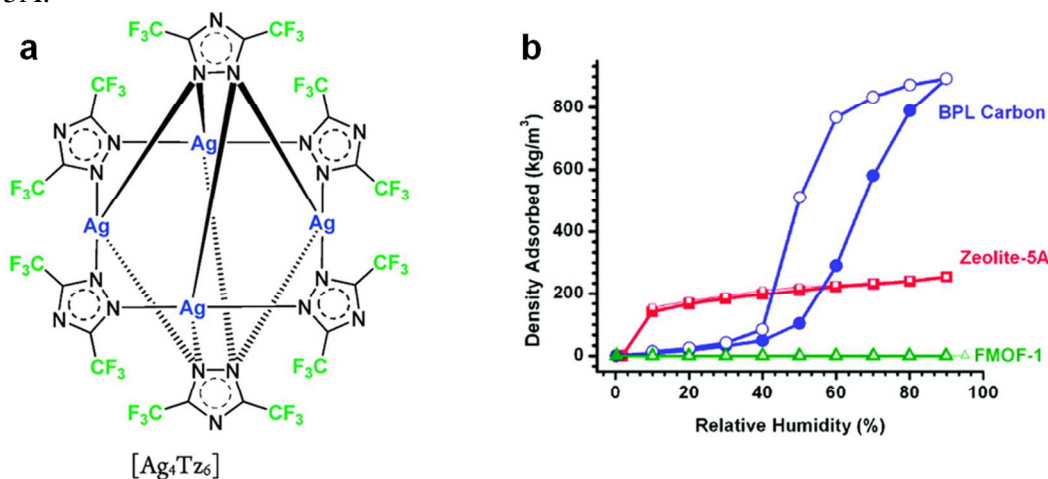


**Figure 9.** Left (a): Building block of FMOF-1 showing  $\text{CF}_3$  groups pointing to the pores, right (b): water adsorption isotherms for FMOF-1 (green), zeolite-5A (red) and BPL Carbon (blue). The figure is reprinted with permission from reference<sup>88</sup>. Copyright (2013), American Chemical Society.

The hydrophobic nature of the FMOF-1 pores presents a possibility for adsorption of hydrocarbons in the presence of water as shown in a recent study by Yang et al.<sup>38</sup> Hydrophobicity of the channel walls was shown to foster formation of water clusters, opening the door for potential study of chemical reactions occurring in the atmosphere and photochemical reaction in a confined environment.<sup>88</sup> *ab initio* calculations<sup>88</sup> showed the formation of different size water clusters as shown in Figure 10. VdW-DF calculations also confirmed the weak interaction of water with the fluorinated pores and the stability of water clusters. The calculated binding energy of water molecules with the wall is less than  $-46 \text{ kJ/mol}$  and depends on how many water molecules are in the cluster.<sup>88</sup> The cluster stability was found to increase with cluster size and to be further stabilized within the FMOF-1 pores compared to its free form.

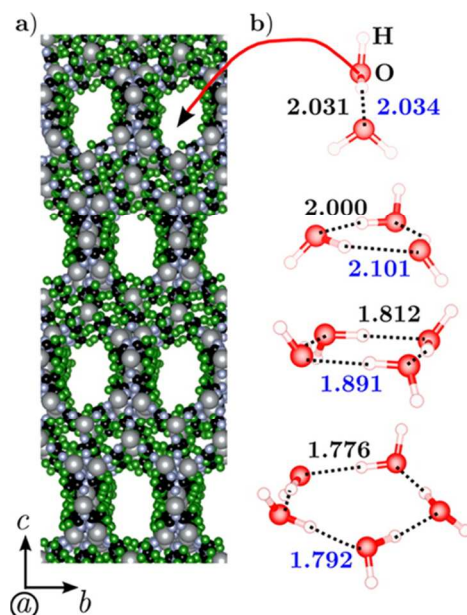


**Figure 10.** Scheme representing water clusters studied by vdW-DF in FMOF-1. The figure is reprinted with permission from reference<sup>88</sup>. Copyright (2013), American Chemical Society.

Water cluster formation and stability in the FMOF-1 pores was studied experimentally using IR absorption spectroscopy. Yang et al<sup>36</sup> studied adsorption of N<sub>2</sub> and H<sub>2</sub> in FMOF-1 showing structural changes with gas incorporation. Water adsorption in FMOF-1 was found to induce changes in the vibrational modes of the framework, indicating slight structural changes a result of water incorporation.<sup>88</sup> Isolated water molecules were also detected, presumed to be in the “micropore” of FMOF-1, i.e. the small cages of the framework, in addition to the water clusters in the main channels.

VdW-DF calculations could not account for water incorporation into the “micropore”; however, changes in the framework structure may allow water incorporation in the micropore because of the flexible nature of the framework. Figure 11 shows the IR absorption spectra of FMOF-1 upon exposures of 0.8, 1, 3 Torr water (bottom panel) and at 15 Torr water (top panel). The sharp IR absorption mode at 3683 cm<sup>-1</sup> was attributed to isolated water adsorbed in the micropore, while the broad absorption modes centered at 3215 and 3371 cm<sup>-1</sup> were assigned to the symmetric and asymmetric OH stretch mode of hydrogen-bonded water. IR absorption modes at 1608 and 1630 cm<sup>-1</sup> were assigned to  $\delta$ (OH) bending modes of isolated and hydrogen bonded water, respectively, and used to quantify the concentration because their intensity is not affected by hydrogen bonding, as is the case of the stretching modes.

The stability of the water clusters in FMOF-1 was studied by monitoring the intensity of the IR absorption modes of water as a function of desorption time (Figure 12). Figure 12 shows the integrated areas of the  $\delta$ (OH) bending modes of water as a function of pressure. The IR intensity of the bending mode attributed to isolated water decreased much more than that of hydrogen-bonded water, an indication of the stability of water clusters in FMOF-1 pores. Moreover, as the water is pushed out of the micropore it contributes to hydrogen-bonded water in the main channel, observed as an increase in the 1676 cm<sup>-1</sup> peak intensity.

In conclusion, the hydrophobic cavities can be used to encapsulate water clusters that can be further explored for chemical reactions in constrained environments.

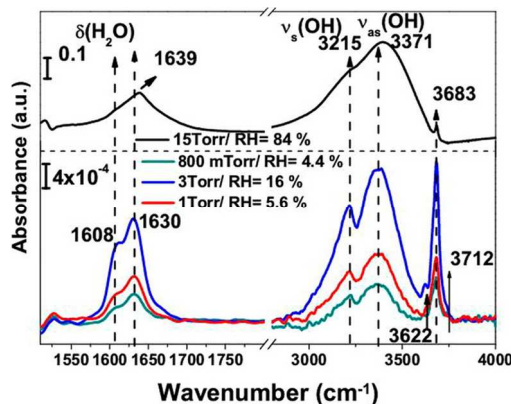


**Figure 11.** IR absorption spectra of FMOF-1 as a function of water vapor pressure. The figure is reprinted with permission from reference <sup>88</sup>. Copyright (2013) American Chemical Society.

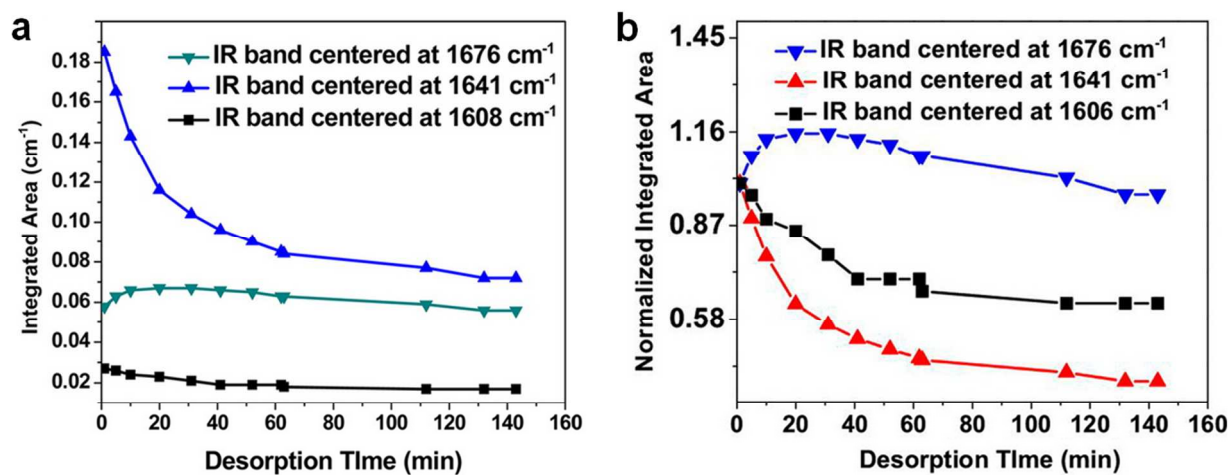


**Figure 12.** Left (a): Integrated area of the bending mode of water in FMOF-1 as a function of desorption time, right (b): Normalized integrated areas to the largest value of the bending mode of adsorbed water. The figure is reprinted with permission from reference <sup>88</sup>. Copyright (2013) American Chemical Society.

#### 4.2. Installing protective groups and influence on stability

In addition to improve the stability of MOFs in moisture environment by modifying the linkers to have a hydrophobic character, there are other ways to make the MOFs to achieve a much stronger tolerance of water molecules by installing protective groups to MOFs. For example, through treating the Cu-BTC (1,3,5 benzenetricarboxylic acid, BTC) or HKUST-1 with a plasma-enhanced chemical vapor deposition (PECVD) of perfluorohexane (PFH), the CuBTC plasma can maintain the structure unchanged even upon immersion in water for a whole day.<sup>89</sup> Although the nitrogen isotherms show that the surface area of Cu-BTC plasma decreases 25.9% and the pore volume decreases 31.7%, the capacity of Cu-BTC plasma was not decreased. In contrast, a larger amount of  $\text{NH}_3$  can be adsorbed on the Cu-BTC plasma. The enhancement of stability of Cu-BTC plasma is attributed to that PFH prevents the collapsing of pores by

hindering water molecules adsorption and impeding water molecules to form large clusters (see Figure 13).

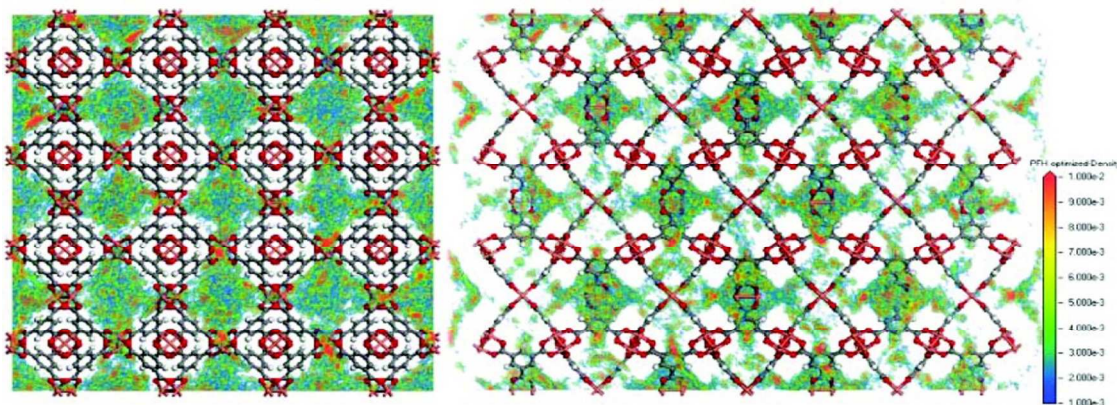


**Figure 13.** GCMC simulations of the adsorption of PFH in Cu-BTC viewed along the [100] (left) and [110] (right) directions. The figure is reprinted with permission from reference<sup>89</sup>. Copyright (2012) American Chemical Society.

Except for PFH, other functional groups can be used to adjust the water stability of MOFs. It is demonstrated that nonpolar groups (e.g. methyl) placing on the bdc ligand of zinc paddlewheel MOFs enhances their water tolerance significantly compared to the parent structure.<sup>39</sup> As a result, even at ~ 90% relative humidity (RH), water molecules will not lead to a loss of crystallinity of the MOFs. However, polar functional groups (e.g. nitro, bromo hydroxy) will facilitate hydrolysis of the Zn-O bond in the MOFs. Molecular simulation in the later study<sup>42</sup> shows that the kinetic stability is enhanced by shielding the carboxylate groups and preventing hydrogen bonding. Protecting the unsaturated metal centers by installing functional groups for enhancing CO<sub>2</sub> selectivity was reported in a recent work by McDonald et al.<sup>90</sup> The work presents functionalization of M<sub>2</sub>(dobpdc) (M=Zn, Mg; dobpdc<sup>4-</sup>=4,4'-dioxido-3,3'-biphenyldicarboxylate), forming an expanded MOF-74 structure type with N,N'-dimethylethylenediamine (mmen) to afford Mg<sub>2</sub>(dobpdc)(mmen)<sub>1.6</sub>(H<sub>2</sub>O)<sub>0.4</sub> (mmen-Mg<sub>2</sub>(dobpdc)).

Another kind of MOFs (Banasorb-22), which has a similar structure with MOF-5, was shown to have much stronger stability in moist environments. Even after exposure to boiling water steam for one week, only minor changes of its structure were observed.<sup>40</sup> Such strong water stability was attributed to the incorporation of a water-repellant group, trifluoromethoxy substituent, by modification of the terephthalic acid linkers before synthesis. With a similar approach based on postsynthetic covalent modification (PSM) with long alkyl groups in IRMOF-3, Nguyen and co-workers were also able to transform this moisture-sensitive MOFs into a water resistant material.<sup>91</sup>

#### 4.3. Zr-MOFs

Besides employing functional groups to prevent water molecules from destroying the MOFs' structure, another effective way to enhance the chemical stability of MOFs in moisture is to replace the metal used to connect the organic linkers. One notable example is Zr-based MOFs

UiO-66 developed by Cavka and co-workers,<sup>37</sup> which contains the robust  $Zr_6O_4(OH)_4(CO_2)_{12}$  cluster units with a full 12 metal coordination configuration. With this basic structure, it was shown that the length of the linkers could be increased without compromising the material stability. Furthermore, it was found that the weakest bond in the structure is no longer the connection between the linker and the metal atoms. Instead, the bond between the benzene rings and the terminal carboxyl group is the easiest one to break. As a result, these kinds of MOFs have good thermal and chemical stability.

Furthermore, the UiO-66 MOF can be modified with many functional groups such as amino ( $-NH_2$ ), nitro ( $-NO_2$ ), methoxy ( $-OMe$ ), and naphthyl ( $-Naphyl$ ) to improve gas adsorption selectivity and inhibit water adsorption in UiO-66-1,4-Naphyl.<sup>39, 43</sup>

Several kinds of zirconium MOFs are synthesized by connecting  $Zr_6O_4(OH)_4(-CO_2)_n$  secondary building units and variously shaped carboxyl organic linkers (e.g. fumaric acid, -BDC, -MTB, -BTC, etc.).<sup>25</sup> Figure 14a shows the crystal structure of MOF-841 prepared with MTB (4, 4', 4'', 4'''-Methanetetrayltetrabenzoic acid) as the linker. These zirconium-based MOFs exhibit a steep water uptake capacity (see Figure 14) and high cycling performance, which means lower energy is required to recycle the MOFs. Even after five adsorption/desorption cycles (see Figure 14b), no significant loss of its water adsorption capacity was observed and the regeneration process could be performed at room temperature. Such good water stability can be attributed to the specific pore size and the hydrogen bonds formed between water molecules and the zirconium SBUs

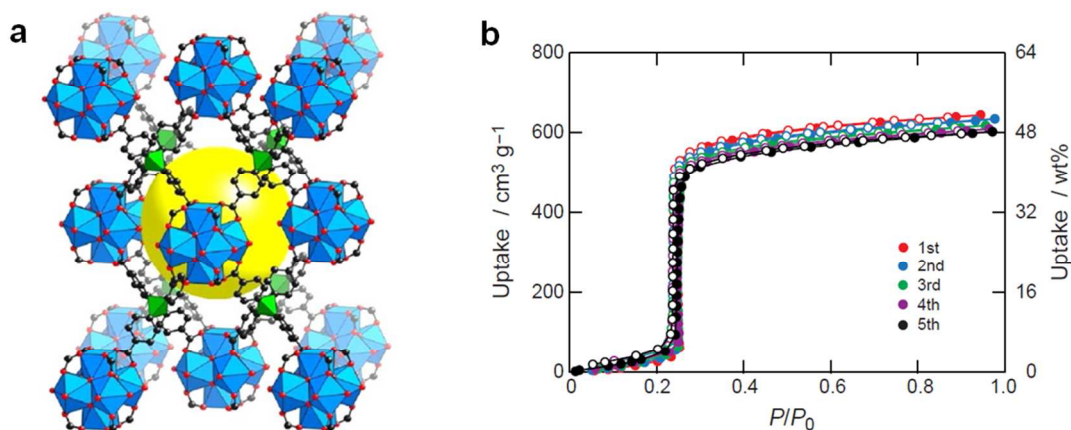


**Figure 14.** Right (a): Structure of MOF-841; and Right (b): Cycle performance of water uptake in MOF-841 at 25 °C. The figure is reprinted with permission from reference<sup>25</sup>. Copyright (2014) American Chemical Society.

In addition to the modification of the organic linkers or the strengthening of the metal-ligand bonds by using  $Zr^{4+}$  cations, there have been other reports of water stable MOFs. For example, some MOFs structures with porphyrin ligand as building block do not only exhibit biomimetic or photocatalytic activity but also remain quite stable even in aqueous acid/base conditions.<sup>92-96</sup> A 2-fold interpenetrated microporous framework  $[Ni_2(C_2O_4)(L)_2]_n \cdot 6nH_2O$ , synthesized by a new ligand  $L=4,2':4'',2'$ -terpyridine-4'-carboxylic acid, also retains its structure in hot water.<sup>97</sup> Taddei and co-workers<sup>98</sup> reported that Tubular MOFs based on copper(II) phosphinates and bipyridine

remain stable in boiling water. In contrast, another structurally similar MOFs built with a 1,2-bis(4-pyridyl)ethane ligand slowly transforms into another stable strip phase when placed in water. The high stability of the former MOFs was attributed to the fact that no other more stable structures are possible by reaction with water.<sup>98</sup> Imidazolate-bridged frameworks show remarkable chemical resistance,<sup>19, 20, 99</sup> attributed to the high  $pK_a$  of imidazolate that tends to increase the metal-N bond strength within the frameworks. Since pyrazoles have similar high  $pK_a$  values, Long's team developed pyrazolate-bridged MOFs, which have also been shown to be very stable in boiling water, organic solvents, and acidic media.<sup>100</sup> Finally,  $[K(H_2O)_2Co_3(cit)(Hcit)]$  (UTSA-16), constructed by citrate chelating of one cubic  $(Co(2)_4O_4)$  cluster, two Co(1) tetrahedral and two K ions, displays repeatable and reversible high  $CO_2$  uptake ( $160 \text{ cm}^3 \text{ cm}^{-3}$ ) at ambient conditions. While the  $CO_2$  uptake in these compounds is slightly lower than in Mg-MOF-74 ( $162 \text{ cm}^3 \text{ cm}^{-3}$ ), they are more stable in air than any MOF-74 compound.<sup>101</sup>

## 5. Conclusions

The mechanism of water interaction with metal organic frameworks has been discussed in this highlight by focusing first on two representative MOFs:  $M(bdc)(ted)_{0.5}$  and MOF-74 hydration process. In both cases, water molecules were found to preferentially attack the metal-ligand nodes, either hydrolyzing metal-oxygen groups or displacing the ligands. The stability and decomposition reaction pathway of MOFs upon exposure to water vapor critically depends on their structure and the specific metal cation in the building units. For instance, in  $M(bdc)(ted)_{0.5}$ , the metal-bdc bond is the most vulnerable for  $Cu(bdc)(ted)_{0.5}$ , while the metal-ted bond is first attacked for the Zn and Co analogs. In contrast,  $Ni(bdc)(ted)_{0.5}$  remains stable under conditions where all other  $M(bdc)(ted)_{0.5}$  materials are chemically attacked. In the case of  $M_2(dobdc)$ , or MOF-74, the weak link is the phenolate-metal bond. The water molecule dissociatively adsorbs at the metal-oxygen group with OH or OD attached directly on the metal center and the H or D atoms bonded to oxygen atoms of phenol group. Interestingly, the latter O-H bond is only detected when  $D_2O$  is used. When  $H_2O$  is used, the IR experiments are not able to detect the fingerprint of the water dissociation due to the strong vibrational coupling of the O-H bending vibration to the dobdc linker vibrations. In contrast, the O-D bending vibration is fully decoupled from the linker vibrations (i.e. behaves as a local vibrational mode) leading to a strong, sharp and detectable absorption band.

This type of detailed information is important to develop strategies for protecting the metal-ligand node or improving the metal-ligand bond strength to resist reaction with water. A good number of successful examples such as fluorinated MOFs, Zr-MOFs and MOFs with water repellent groups have been found in the literatures and inspires more efforts to develop water stable MOFs.

## Acknowledgement

This work was entirely supported by the Department of Energy Grant No. DE-FG02-08ER46491.

## Reference:

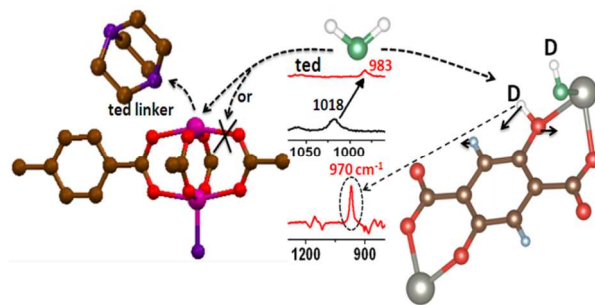
1. H. Wu, Q. Gong, D. H. Olson and J. Li, *Chem. Rev.*, 2012, **112**, 836-868.
2. H.-C. Zhou, J. R. Long and O. M. Yaghi, *Chem. Rev.*, 2012, **112**, 673-674.

3. M. P. Suh, H. J. Park, T. K. Prasad and D.-W. Lim, *Chem. Rev.*, 2011, **112**, 782-835.
4. J.-R. Li, J. Sculley and H.-C. Zhou, *Chem. Rev.*, 2011, **112**, 869-932.
5. K. Sumida, D. L. Rogow, J. A. Mason, T. M. McDonald, E. D. Bloch, Z. R. Herm, T.-H. Bae and J. R. Long, *Chem. Rev.*, 2011, **112**, 724-781.
6. R. J. Kuppler, D. J. Timmons, Q.-R. Fang, J.-R. Li, T. A. Makal, M. D. Young, D. Yuan, D. Zhao, W. Zhuang and H.-C. Zhou, *Coord. Chem. Rev.*, 2009, **253**, 3042-3066.
7. G. Férey, *Chem. Soc. Rev.*, 2008, **37**, 191-214.
8. O. Shekhah, H. Wang, D. Zacher, R. A. Fischer and C. Wöll, *Angew. Chem. Int. Ed.*, 2009, **48**, 5038-5041.
9. J. S. Seo, D. Whang, H. Lee, S. I. Jun, J. Oh, Y. J. Jeon and K. Kim, *Nature*, 2000, **404**, 982-986.
10. G. Férey, M. Latroche, C. Serre, F. Millange, T. Loiseau and A. Percheron-Guegan, *Chem. Commun.*, 2003, 2976-2977.
11. G. Férey, C. Mellot-Draznieks, C. Serre, F. Millange, J. Dutour, S. Surblé and I. Margiolaki, *Science*, 2005, **309**, 2040-2042.
12. J.-R. Li, R. J. Kuppler and H.-C. Zhou, *Chem. Soc. Rev.*, 2009, **38**, 1477-1504.
13. D. P. Broom and K. M. Thomas, *MRS Bull.*, 2013, **38**, 412-421.
14. H. Wu, W. Zhou and T. Yildirim, *J. Am. Chem. Soc.*, 2009, **131**, 4995-5000.
15. L. Huang, H. Wang, J. Chen, Z. Wang, J. Sun, D. Zhao and Y. Yan, *Microporous Mesoporous Mater.*, 2003, **58**, 105-114.
16. Y. Li and R. T. Yang, *Langmuir*, 2007, **23**, 12937-12944.
17. J. B. DeCoste, G. W. Peterson, B. J. Schindler, K. L. Killops, M. A. Browe and J. J. Mahle, *J. Mater. Chem.*, 2013, **1**, 11922-11932.
18. A. C. Kizzie, A. G. Wong-Foy and A. J. Matzger, *Langmuir*, 2011, **27**, 6368-6373.
19. K. S. Park, Z. Ni, A. P. Côté, J. Y. Choi, R. Huang, F. J. Uribe-Romo, H. K. Chae, M. O'Keeffe and O. M. Yaghi, *Proceedings of the National Academy of Sciences*, 2006, **103**, 10186-10191.
20. A. Demessence, D. M. D'Alessandro, M. L. Foo and J. R. Long, *J. Am. Chem. Soc.*, 2009, **131**, 8784-8786.
21. R. S. Haszeldine, *Science*, 2009, **325**, 1647-1652.
22. J. Canivet, A. Fateeva, Y. Guo, B. Coasne and D. Farrusseng, *Chem. Soc. Rev.*, 2014.
23. P. Küsgens, M. Rose, I. Senkovska, H. Fröde, A. Henschel, S. Siegle and S. Kaskel, *Microporous Mesoporous Mater.*, 2009, **120**, 325-330.
24. J. Canivet, J. Bonnefoy, C. Daniel, A. Legrand, B. Coasne and D. Farrusseng, *New J. Chem.*, 2014, **38**, 3102-3111.
25. H. Furukawa, F. Gándara, Y.-B. Zhang, J. Jiang, W. L. Queen, M. R. Hudson and O. M. Yaghi, *J. Am. Chem. Soc.*, 2014, **136**, 4369-4381.
26. J. J. Low, A. I. Benin, P. Jakubczak, J. F. Abrahamian, S. A. Faheem and R. R. Willis, *J. Am. Chem. Soc.*, 2009, **131**, 15834-15842.
27. D. Saha and S. Deng, *J. Phys. Chem. Lett.*, 2009, **1**, 73-78.
28. K. A. Cychoz and A. J. Matzger, *Langmuir*, 2010, **26**, 17198-17202.
29. I. J. Kang, N. A. Khan, E. Haque and S. H. Jung, *Chem. Eur. J.*, 2011, **17**, 6437-6442.
30. K. Tan, N. Nijem, P. Canepa, Q. Gong, J. Li, T. Thonhauser and Y. J. Chabal, *Chem. Mater.*, 2012, **24**, 3153-3167.
31. J. B. DeCoste, G. W. Peterson, H. Jasuja, T. G. Glover, Y.-g. Huang and K. S. Walton, *J. Mater. Chem. A*, 2013, **1**, 5642-5650.
32. M. Dion, H. Rydberg, E. Schröder, D. C. Langreth and B. I. Lundqvist, *Phys. Rev. Lett.*, 2004, **92**, 246401.
33. T. Thonhauser, V. R. Cooper, S. Li, A. Puzder, P. Hyldgaard and D. C. Langreth, *Phys. Rev. B*, 2007, **76**, 125112.
34. D. C. Langreth, B. I. Lundqvist, S. D. Chakarova-Kack, V. R. Cooper, M. Dion, P. Hyldgaard, A. Kelkkanen, J. Kleis, L. Kong, S. Li, P. G. Moses, E. Murray, A. Puzder, H. Rydberg, E. Schroder and T. Thonhauser, *J. Phys.: Condens. Matter.*, **2009**, **21**, 084203.

35. S. Zuluaga, P. Canepa, K. Tan, Y. J. Chabal and T. Thonhauser, *J. Phys.: Condens. Matter*, 2014, **26**, 133002.
36. C. Yang, X. Wang and M. A. Omary, *J. Am. Chem. Soc.*, 2007, **129**, 15454-15455.
37. J. H. Cavka, S. Jakobsen, U. Olsbye, N. Guillou, C. Lamberti, S. Bordiga and K. P. Lillerud, *J. Am. Chem. Soc.*, 2008, **130**, 13850-13851.
38. C. Yang, U. Kaipa, Q. Z. Mather, X. Wang, V. Nesterov, A. F. Venero and M. A. Omary, *J. Am. Chem. Soc.*, 2011, **133**, 18094-18097.
39. H. Jasuja, Y.-g. Huang and K. S. Walton, *Langmuir*, 2012, **28**, 16874-16880.
40. T. Wu, L. Shen, M. Luebbbers, C. Hu, Q. Chen, Z. Ni and R. I. Masel, *Chem. Commun.*, 2010, **46**, 6120-6122.
41. J. M. Taylor, R. Vaidhyanathan, S. S. Iremonger and G. K. H. Shimizu, *J. Am. Chem. Soc.*, 2012, **134**, 14338-14340.
42. H. Jasuja, N. C. Burtch, Y.-g. Huang, Y. Cai and K. S. Walton, *Langmuir*, 2012, **29**, 633-642.
43. M. Kandiah, S. Usseglio, S. Svelle, U. Olsbye, K. P. Lillerud and M. Tilset, *J. Mater. Chem.*, 2010, **20**, 9848-9851.
44. J. H. Im, N. Ko, S. J. Yang, H. J. Park, J. Kim and C. R. Park, *New J. Chem.*, 2014, **38**, 2752-2755.
45. J. A. Greathouse and M. D. Allendorf, *J. Am. Chem. Soc.*, 2006, **128**, 10678-10679.
46. J. Y. Lee, D. H. Olson, L. Pan, T. J. Emge and J. Li, *Adv. Funct. Mater.*, 2007, **17**, 1255-1262.
47. K. Tan, P. Canepa, Q. Gong, J. Liu, D. H. Johnson, A. Dyevoich, P. K. Thallapally, T. Thonhauser, J. Li and Y. J. Chabal, *Chem. Mater.*, 2013, **25**, 4653-4662.
48. Y. F. Chen, J. Y. Lee, R. Babarao, J. Li and J. W. Jiang, *J. Phys. Chem. C.*, 2010, **114**, 6602-6609.
49. Z. Liang, M. Marshall and A. L. Chaffee, *Microporous Mesoporous Mater.*, 2010, **132**, 305-310.
50. J. Liu, A. I. Benin, A. M. B. Furtado, P. Jakubczak, R. R. Willis and M. D. LeVan, *Langmuir*, 2011, **27**, 11451-11456.
51. P. M. Schoenecker, C. G. Carson, H. Jasuja, C. J. J. Flemming and K. S. Walton, *Ind. Eng. Chem. Res.*, 2012, **51**, 6513-6519.
52. P. D. C. Dietzel, R. E. Johnsen, H. Fjellvag, S. Bordiga, E. Groppo, S. Chavan and R. Blom, *Chem. Commun.*, 2008, 5125-5127.
53. A. C. McKinlay, B. Xiao, D. S. Wragg, P. S. Wheatley, I. L. Megson and R. E. Morris, *J. Am. Chem. Soc.*, 2008, **130**, 10440-10444.
54. K. Yu, K. Kiesling and J. R. Schmidt, *J. Phys. Chem. C.*, 2012, **116**, 20480-20488.
55. N. Nijem, J.-F. Veyan, L. Kong, H. Wu, Y. Zhao, J. Li, D. C. Langreth and Y. J. Chabal, *J. Am. Chem. Soc.*, 2010, **132**, 14834-14848.
56. H. Furukawa, K. E. Cordova, M. O'Keeffe and O. M. Yaghi, *Science*, 2013, **341**.
57. M. De Toni, R. Jonchiere, P. Pullumbi, F.-X. Coudert and A. H. Fuchs, *ChemPhysChem*, 2012, **13**, 3497-3503.
58. S. S. Han, S.-H. Choi and A. C. T. van Duin, *Chem. Commun.*, 2010, **46**, 5713-5715.
59. A. Vimont, J.-M. Goupil, J.-C. Lavalley, M. Daturi, S. Surblé, C. Serre, F. Millange, G. Férey and N. Audebrand, *J. Am. Chem. Soc.*, 2006, **128**, 3218-3227.
60. A. Vimont, H. Leclerc, F. Maugé, M. Daturi, J.-C. Lavalley, S. Surblé, C. Serre and G. Férey, *J. Phys. Chem. C.*, 2006, **111**, 383-388.
61. H. Chun, D. N. Dybtsev, H. Kim and K. Kim, *Chem. Eur. J.*, 2005, **11**, 3521-3529.
62. S. I. Vagin, A. K. Ott and B. Rieger, *Chem. Eng. Technol.*, 2007, **79**, 767-780.
63. B. Chen, S. Ma, F. Zapata, F. R. Fronczek, E. B. Lobkovsky and H.-C. Zhou, *Inorg. Chem.*, 2007, **46**, 1233-1236.
64. P. Maniam and N. Stock, *Inorg. Chem.*, 2011, **50**, 5085-5097.
65. Y. Zhao, H. Wu, T. J. Emge, Q. Gong, N. Nijem, Y. J. Chabal, L. Kong, D. C. Langreth, H. Liu, H. Zeng and J. Li, *Chem. Eur. J.*, 2011, **17**, 5101-5109.

66. B. Kozlevčar, I. Leban, M. Petrič, S. Petriček, O. Roubeau, J. Reedijk and P. Šegedin, *Inorg. Chim. Acta*, 2004, **357**, 4220-4230.
67. N. Benbellat, K. S. Gavrilenko, Y. Le Gal, O. Cador, S. Golhen, A. Gouasmia, J.-M. Fabre and L. Ouahab, *Inorg. Chem.*, 2006, **45**, 10440-10442.
68. P. Song, Y. Li, B. He, J. Yang, J. Zheng and X. Li, *Microporous Mesoporous Mater.*, 2011, **142**, 208-213.
69. N. Nijem, J.-F. Veyan, L. Kong, K. Li, S. Pramanik, Y. Zhao, J. Li, D. Langreth and Y. J. Chabal, *J. Am. Chem. Soc.*, 2010, **132**, 1654-1664.
70. X. Wang and L. Andrews, *Inorg. Chem.*, 2005, **44**, 9076-9083.
71. S. G. Stepanian, I. D. Reva, E. D. Radchenko and G. G. Sheina, *Vib. Spectrosc.*, 1996, **11**, 123-133.
72. D. Hadzi and N. Sheppard, *Proc. R. Soc. A.*, 1953, **A216**, 247-267.
73. J. F. Arenas and J. I. Marcos, *Spectrochim. Acta Mol. Spectros.*, 1979, **35**, 355-363.
74. C. Prestipino, L. Regli, J. G. Vitillo, F. Bonino, A. Damin, C. Lamberti, A. Zecchina, P. L. Solari, K. O. Kongshaug and S. Bordiga, *Chem. Mater.*, 2006, **18**, 1337-1346.
75. Y. Mathey, D. R. Greig and D. F. Shriver, *Inorg. Chem.*, 1982, **21**, 3409-3413.
76. D. A. Guzonas and D. E. Irish, *Can. J. Chem.*, 1988, **66**, 1249-1257.
77. D. A. Guzonas, D. E. Irish and G. F. Atkinson, *Langmuir*, 1989, **5**, 787-796.
78. D. E. Irish, D. Guzonas and G. F. Atkinson, *Surf. Sci.*, 1985, **158**, 314-324.
79. H. Li, M. Eddaoudi, T. L. Groy and O. M. Yaghi, *J. Am. Chem. Soc.*, 1998, **120**, 8571-8572.
80. H. F. Clausen, R. D. Poulsen, A. D. Bond, M.-A. S. Chevallier and B. B. Iversen, *J. Solid State Chem.*, 2005, **178**, 3342-3351.
81. D. R. Lide, *CRC Handbook of Chemistry and Physics, 89th ed.*; CRC Press: Boca Raton, FL, 2009.
82. L. G. Sillen and A. E. Martell, *Lange's Handbook; The Chemical Society: London*, 1964.
83. A. O. z. r. Yazaydin, R. Q. Snurr, T.-H. Park, K. Koh, J. Liu, M. D. LeVan, A. I. Benin, P. Jakubczak, M. Lanuza, D. B. Galloway, J. J. Low and R. R. Willis, *J. Am. Chem. Soc.*, 2009, **131**, 18198-18199.
84. Y. Liu, H. Kabbour, C. M. Brown, D. A. Neumann and C. C. Ahn, *Langmuir*, 2008, **24**, 4772-4777.
85. K. Tan, S. Zuluaga, Q. Gong, P. Canepa, T. Thonhauser, J. Li and Y. J. Chabal, *Under reviewed by J. Am. Chem. Soc.*, 2014.
86. P. Canepa, C. A. Arter, E. M. Conwill, D. H. Johnson, B. A. Shoemaker, K. Z. Soliman and T. Thonhauser, *J. Mater. Chem. A*, 2013, **1**, 13597-13604.
87. T. A. Makal, X. Wang and H.-C. Zhou, *Cryst. Growth Des.*, 2013, **13**, 4760-4768.
88. N. Nijem, P. Canepa, U. Kaipa, K. Tan, K. Roodenko, S. Tekarli, J. Halbert, I. W. H. Oswald, R. K. Arvapally, C. Yang, T. Thonhauser, M. A. Omary and Y. J. Chabal, *J. Am. Chem. Soc.*, 2013, **135**, 12615-12626.
89. J. B. Decoste, G. W. Peterson, M. W. Smith, C. A. Stone and C. R. Willis, *J. Am. Chem. Soc.*, 2012, **134**, 1486-1489.
90. T. M. McDonald, W. R. Lee, J. A. Mason, B. M. Wiers, C. S. Hong and J. R. Long, *J. Am. Chem. Soc.*, 2012, **134**, 7056-7065.
91. J. G. Nguyen and S. M. Cohen, *J. Am. Chem. Soc.*, 2010, **132**, 4560-4561.
92. A. Fateeva, P. A. Chater, C. P. Ireland, A. A. Tahir, Y. Z. Khimiyak, P. V. Wiper, J. R. Darwent and M. J. Rosseinsky, *Angew. Chem.*, 2012, **124**, 7558-7562.
93. D. Feng, W.-C. Chung, Z. Wei, Z.-Y. Gu, H.-L. Jiang, Y.-P. Chen, D. J. Darensbourg and H.-C. Zhou, *J. Am. Chem. Soc.*, 2013, **135**, 17105-17110.
94. L. Xu, J. Wang, Y. Xu, Z. Zhang, P. Lu, M. Fang, S. Li, P. Sun and H.-K. Liu, *CrystEngComm*, 2014, **16**, 8656-8659.
95. H.-L. Jiang, D. Feng, K. Wang, Z.-Y. Gu, Z. Wei, Y.-P. Chen and H.-C. Zhou, *J. Am. Chem. Soc.*, 2013, **135**, 13934-13938.

96. D. Feng, Z.-Y. Gu, J.-R. Li, H.-L. Jiang, Z. Wei and H.-C. Zhou, *Angew. Chem. Int. Ed.*, 2012, **51**, 10307-10310.
97. Y. Li, Z. Ju, B. Wu and D. Yuan, *Crystal Growth & Design*, 2013, **13**, 4125-4130.
98. M. Taddei, A. Ienco, F. Costantino and A. Guerri, *RSC Advances*, 2013, **3**, 26177-26183.
99. R. Banerjee, A. Phan, B. Wang, C. Knobler, H. Furukawa, M. O'Keeffe and O. M. Yaghi, *Science*, 2008, **319**, 939-943.
100. H. J. Choi, M. Dinca, A. Dailly and J. R. Long, *Energy Environ Sci*, 2010, **3**, 117-123.
101. S. Xiang, Y. He, Z. Zhang, H. Wu, W. Zhou, R. Krishna and B. Chen, *Nat Commun*, 2012, **3**, 954.



Insight into the structural variation of metal organic frameworks materials upon hydration